Proceedings of the 4th International Conference on Software Engineering and Machine Learning
DOI: 10.54254/2755-2721/2026.33981

Research on the Design and Optimization of a Multimodal Data Acquisition System for Drones in Complex Urban Environments

Siwei Han

Institute of Innovative Engineering, Macau University of Science and Technology, Macao, China
1230005656@student.must.edu.mo

Abstract. Amid the rapid rollout of smart city programs, drones have emerged as an indispensable platform for acquiring urban spatial information. Yet within built-up urban settings—crowded with high-rise structures, marked by pronounced GNSS signal blockage, and shaped by complicated airflow regimes—the conventional single-sensor data acquisition approach falls short of satisfying, at the same time, the requirements for precision, operational efficiency, and data completeness.To cope with the intricacies of urban built environments, this paper advances a multi-modal drone-based data acquisition system. At the hardware level, a platform integrating LiDAR, visible-spectrum cameras, and high-accuracy positioning modules is constructed. On top of that sensing stack, a spatiotemporal synchronization calibration method is introduced, built around hardware triggering and timestamp alignment .From the planning side, an adaptive path-design strategy that embeds data-quality indicators is proposed. Specifically, a multi-objective optimization model is formulated to jointly account for path length, obstacle-avoidance safety, and data acquisition quality. Once environmental changes arise, a dynamic replanning mechanism is activated, drawing on the elite-initialization idea from multi-strategy artificial swarm algorithms to raise search efficiency; third-order B-spline curves, meanwhile, are used to smooth the resulting trajectories so that dynamic constraints are satisfied. Not limited to single-platform operation, the system also includes a multi-drone collaborative acquisition mechanism, where distributed task allocation is achieved through a market-auction scheme and acquisition efficiency, together with data consistency, is strengthened through a hierarchical collaborative obstacle-avoidance framework.

Keywords: drone, multimodal data, path planning, multi-drone collaboration, complex urban environment, sensor fusion

1. Introduction

Drones are now the dominant platform for acquiring urban spatial information, with routine deployment across smart-city systems, real-scene 3D reconstruction, and security inspection tasks. Yet urban environments are difficult measurement spaces. Within "urban canyons" created by dense high-rise building clusters, GNSS signals are often lost; for real-world 3D modeling, point-cloud

© 2026 The Authors. This is an open access article distributed under the terms of the Creative Commons Attribution License 4.0 (https://creativecommons.org/licenses/by/4.0/).

DOI: 10.54254/2755-2721/2026.33981

densities of at least 100 points/m² and image overlap rates of at least 80% are required [1], thresholds that conventional flight-path designs often fail to satisfy [2]; at larger collection scales, coordinated operation among multiple drones becomes necessary, but manual planning remains inefficient and is easily accompanied by coverage gaps. Taken together, these constraints place new demands on drone-based acquisition systems: adaptability to complex environments, assured data quality, and higher operational efficiency.

Drone acquisition technology has progressed from single-sensor configurations to multimodal fusion architectures, and from manually mediated remote operation to autonomous flight. In the domain of sensor integration, the DJI M300, paired with LiDAR and an oblique camera, has effectively emerged as a mainstream configuration.

As for calibration, Zhang et al. introduced a grid-based calibration method [3] that exploits geometric constraints shared by the same grid plane in LiDAR point clouds and camera images, thereby estimating rotational and translational parameters through observation of a planar grid. Along a related technical line, Geiger et al. developed the Kalibr toolkit for joint spatiotemporal calibration of cameras and IMUs [4]. In path planning, A* and RRT algorithms perform reliably in relatively simple environments [5]; once the setting shifts into complex three-dimensional space, however, computational efficiency deteriorates. To address that trade-off, multi-objective evolutionary algorithms, including NSGA-II, have been brought in to balance path length against obstacle-avoidance safety. With respect to quality control, standards are already in place for point-cloud indicators such as integrity, accuracy, and density, whereas overlap-rate control continues to depend on equidistant flight-path design, without an adaptive adjustment mechanism.

Over the past several years, work on GigaVision, that is, 10-billion-pixel visual intelligence, has accelerated noticeably. Within the GigaMVS dataset, the covered spatial extent ranges from several thousand to several tens of thousands of square meters [6], a scale that places simultaneous demands on the acquisition pipeline: macroscopic scene organization must be recorded, yet microscopic detail cannot be sacrificed. By contrast, most currently available datasets have been collected through fixed camera arrays or ground-based scanning setups, and with that design choice comes an obvious limitation, namely, the absence of the operational flexibility afforded by drone platforms. For precisely that reason, this system furnishes dependable support for data acquisition in this line of research.

Considered as a whole,drone-based data acquisition has indeed progressed substantially in sensor integration,path planning,and quality-control procedures; even so,several constraints remain unresolved in complex urban settings—above all,weak collaborative mechanisms for multimodal data acquisition,insufficient coupling between path-planning strategies and data-quality metrics,and the lack of systematic validation at the field level. Set against this problem context,the present paper advances a drone-based multimodal data acquisition system tailoblue specifically to complex urban environments and,in parallel,conducts a broad investigation spanning system design,path optimization,multi-drone coordination,and quality assessment,the stated aim being to improve acquisition efficiency as well as the quality of the data ultimately produced.

1.1. Main research content of this paper

This paper puts forward an adaptive path-planning and multi-drone collaborative acquisition method that explicitly embeds data-quality metrics,producing four main outcomes. As a first outcome,a multimodal acquisition hardware system was developed,covering drone-platform selection,multi-sensor integration,and spatiotemporal synchronization calibration.Second, an adaptive path-planning strategy was examined, with a multi-objective optimization scheme proposed for path generation,

DOI: 10.54254/2755-2721/2026.33981

local dynamic replanning, and trajectory smoothing under data-quality constraints. Third, a multi-drone collaborative acquisition mechanism was constructed, integrating a task-allocation algorithm grounded in a market-auction framework and a hierarchical collaborative obstacle-avoidance replanning algorithm. Finally, system validation and engineering implementation were carried out, including simulations of three representative urban scenarios and comparative performance tests against the A* and ABC algorithms.

1.2. Contributions of this paper

1. A multi-objective path-planning model is proposed in which data-quality metrics are directly incorporated into the optimization formulation, with point-cloud completeness and image-overlap rate embedded as explicit objective terms in the path-selection process.

2. Develop a multi-machine collaborative dynamic replanning mechanism, achieving over 25% improvement in data acquisition efficiency compared to traditional methods.

3. Establish a closed-loop technical process encompassing "system design – path optimization – data fusion – quality evaluation".

2. System design and hardware integration

2.1. Overall architecture of the data acquisition system

2.1.1. UAV platform selection

To satisfy the operational requirements posed by complex urban environmental scenarios, the DJI Jingwei M300 RTK was adopted as the flight platform. Rated for a maximum takeoff weight of 9 kg, the aircraft can accommodate three payloads and, when flown without load, sustain an endurance of 55 minutes. In addition, six-direction obstacle avoidance is supported, and dual-RTK centimeter-level positioning is provided. Real-time data processing and path re-planning are executed by the onboard Miaosuan Manifold 2-G computer, equipped with 512 CUDA cores.

2.1.2. Multimodal sensor configuration

For high-precision 3D reconstruction, the system draws on the following sensor suite: LiDAR, specifically the Livox AVIA, provides a detection range of 450 m (at 80% reflectivity), a 70.4° × 77.2° field of view, and point-cloud density reaching 200 points/m² at 10 m. For visible-spectrum imaging, a Sony ILCE-6000 camera (24 MP) is used, with external triggering supported and a 20 mm prime lens mounted. For positioning, the M300 integrates an RTK+POS module, delivering static accuracy of 5 mm ± 1 ppm while outputting position and attitude data at 200 Hz. Supplementing these components are auxiliary sensors, namely a three-axis IMU and an altimeter.

Cooperative Working Mechanism: Through hardware-triggered timing control, the LiDAR and camera operate in synchronization; by means of PPS-based coordination, the positioning module is temporally aligned with the flight controller and associated sensors so that a unified global time reference is maintained. In urban settings marked by pronounced GNSS occlusion, the multi-sensor fusion scheme yields a marked improvement in positioning robustness [7] (particularly under the sort of signal blockage that tends to destabilize single-source positioning pipelines). Meanwhile, the onboard computing unit handles real-time data acquisition and carries out path re-planning as conditions evolve.

DOI: 10.54254/2755-2721/2026.33981

2.2. Multimodal sensor integration and calibration

2.2.1. Hardware integration solution

The sensors adopt a modular integration scheme and are fixed in place with custom-fabricated carbon-fiber connection plates. At the upper section, the LiDAR and camera are mounted side by side, the LiDAR facing horizontally forward and the camera arranged either vertically downward or at a 45-degree tilt, an orientation choice that permits simultaneous data acquisition from both vertical and ground-view perspectives. At the lower section, the RTK antenna together with the data-transmission module is installed. Through either serial ports or Ethernet connections, all sensors interface with the onboard computer, while PWM trigger signals supplied by the flight controller synchronize the camera shutter with LiDAR rotation. In total, the integrated system weighs 6.8 kg, thus satisfying the payload requirement of the M300.

2.2.2. Spatiotemporal synchronization calibration method

Time synchronization: From the flight controller, one PPS pulse per second is distributed to every sensor, each of which logs its own local timestamp at the instant of reception. Those sensor-side timestamps are then mapped onto a common GPS time base through linear interpolation, with the measured synchronization error remaining below 1 ms.

Spatial calibration is carried out through a hybrid plate-based procedure, by which the rotation matrix and translation vector between the laser radar and the camera are identified. For the purpose of assessing calibration quality, reprojection error is adopted as the evaluation criterion, the average error remaining below 1 pixel (a level generally taken as indicative of tight cross-sensor alignment). For the IMU–laser radar pair, the Kalibr toolbox is used to estimate the extrinsic parameters as well as the associated time delay [8].

3. Path planning and optimization for collection in complex environments

3.1. Scenario modeling and data acquisition requirements analysis

3.1.1. Classification of typical complex urban scenarios

Urban environments are complex, their three-dimensional spatial configurations markedly heterogeneous and their dynamic elements, at times, distinctly random. With targeted path-planning formulation as the operative goal, typical urban scenarios are here classified into three types according to four criteria: building density, degree of spatial openness, GNSS signal quality, and airflow characteristics:

Table 1. Modeling scenario classification

Scene Type	Signalment	Obstacle density	GNSS signal quality	Main challenges in modeling	Priority Goal
High-rise buildings in the canyon area	The building height exceeds 100 meters, and the street is narrow.	high	slightly	Facade cavity, signal loss	Obstacle avoidance safety, point cloud integrity

DOI: 10.54254/2755-2721/2026.33981

Table 1. (continued)

Dense low-rise residential area	The building height ranges from 20 to 50 meters, with a compact layout.	Medium to High	middle	Roof structure, overhead pipelines	Real-time obstacle avoidance, path accessibility
Open squares and public spaces	Broad field of view with sparse obstacles	low	good	Dynamic obstacle avoidance, uniform coverage	Optimal collection efficiency and energy consumption

3.1.2. Data acquisition model for multi-objective optimization

To meet the dual collection requirements of environmental adaptability and quality assurance,the path-planning problem is formulated here as a multi-objective optimization task, explicitly incorporating path cost, threat cost, and data-quality cost [9].

The drone flight trajectory is represented as an ordered sequence of path nodes, P = {Pstart, P1, P2,..., Pend}. For this trajectory, the optimization objective function F is defined as:

$$F=\min(\omega_1*f_{path}+\omega_2*f_{threat}+\omega_3*f_{quality} \quad (1)$$

F: the total cost serving as the optimization objective; lower values correspond to better paths. $\omega_1,\omega_2,\omega_3$: weight coefficients used to balance the relative importance of the three sub-objectives,namely path length,threat level,and data quality. f_{path} : path length cost. f_{threat} : threat cost. $f_{quality}$: data-quality cost.

(1) Path length cost: This term represents the cumulative distance across all path segments and is introduced to blueuce energy consumption.

$$f_{path} = \sum_{i=1}^{n-1} \sqrt{(x_{i+1} - x_i)^2 + (y_{i+1} - y_i)^2 + (z_{i+1} - z_i)^2} \quad (2)$$

n:The total number of nodes on the path, including the starting and ending points.

$x_iy_iz_i$:The 3D coordinates of the i-th path node.

(2) Threat cost: Around nearby obstacles,a safety buffer must be preserved by the drone. Under the potential-field formulation adopted in this study,proximity to obstacles raises the corresponding cost directly; put differently,the smaller the separation distance,the larger the imposed penalty.

$$f_{threat} = \sum_{i=1}^{n} \sum_{j=1}^{M} \frac{K}{(||P_i - O_j||)^2} \quad (3)$$

M:Total number of obstacles in the environment. P_i :The position vector of the i-th path node. O_j :The position vector of the j-th path node (typically the obstacle center or the nearest point). $||P_i-O_j||$:The Euclidean distance from the node to the obstacle.K:The scaling factor is used to adjust the sensitivity of the threat cost.

(3) Data-quality cost: As the central methodological component of this study,this cost metric evaluates the coverage quality of the target region,specifically in terms of point-cloud coverage and image-overlap rate.

$$f_{quality} = 1 - \frac{1}{N} \sum_{k=1}^{N} Q_k \quad (4)$$

N:The total number of grids (or sampling points) to be collected for the target area division.

DOI: 10.54254/2755-2721/2026.33981

Q_k :The coverage quality score for the k-th grid typically ranges from 0 (no coverage or poor quality) to 1 (high-quality coverage), taking into account factors such as line-of-sight, angle, and lighting.

Through this formula,the proportion of grids lacking high-quality coverage is computed; as that proportion increases,so too does the data-quality cost. If all grids receive high-quality coverage,then $f_{quality} = 0$; if none are coveblue,then $f_{quality} = 1$.

3.2. Single-machine adaptive path planning

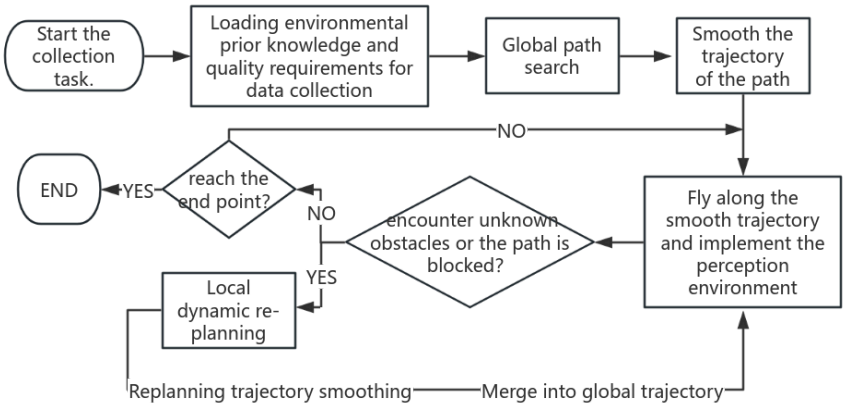


Figure 1. General frame

3.2.1. Global path generation (grounded in an improved RRT* scheme and multi-objective optimization)

In this paper,a hierarchical planning framework is proposed,with three interconnected layers: global path generation,local dynamic re-planning,and trajectory smoothing.

Building on the elite-population initialization and guided-search scheme embedded in the artificial swarm optimization algorithm [10],the present study introduces a multi-strategy guidance mechanism and,on that basis,constructs a hierarchical framework that couples global path generation,local dynamic re-planning,and trajectory smoothing (these three components being treated here as coordinated stages rather than isolated modules). During the sampling phase,more specifically,a quality-guided sampling bias function is deployed so that sampling points are directed toward regions associated with higher data quality,thus enabling multi-objective optimization goals to be incorporated directly into the expansion process. The overall workflow of the proposed multi-objective RRT* algorithm is shown in the figure below.

DOI: 10.54254/2755-2721/2026.33981

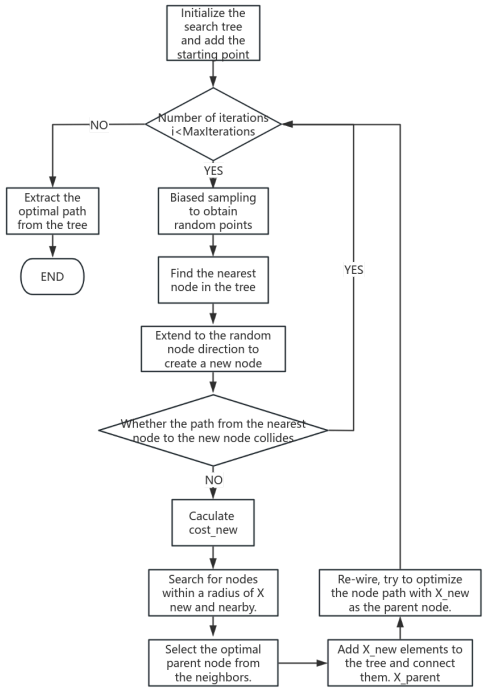


Figure 2. Flowchart of the multi-objective RRT* algorithm

3.2.2. Local dynamic re-planning

Across dense urban airspace,drones routinely deviate from preplanned routes even when nominally tracking globally generated paths,abrupt obstacles such as construction cranes or moving vehicles—as well as broader environmental changes—frequently driving those departures. To address this operational constraint,the present paper adopts the D* Lite algorithm for incremental local replanning. Whenever environmental conditions shift,only the directly affected nodes are updated, rather than the entire path being recomputed from scratch; for real-time airborne applications,that selective update mechanism is particularly well suited.

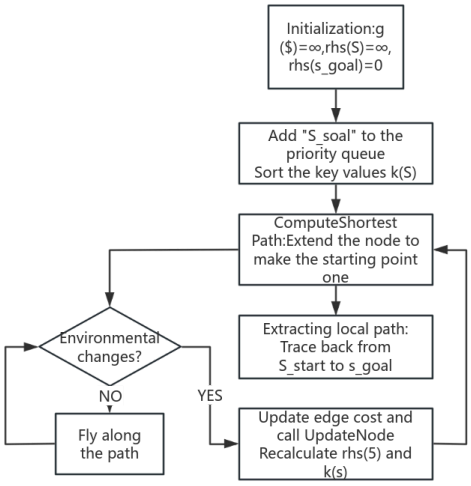


Figure 3. Flowchart of the core algorithm for local dynamic reprogramming

DOI: 10.54254/2755-2721/2026.33981

Among: g(s) Estimation of the current shortest path cost from the starting point to node s. rhs(s) :The heuristic cost at the right end of the node satisfies:

$$\mathrm{rhs(s)}=\min_{\mathrm{s^{'}\in Succ(s)}}(\mathrm{c(s,s^{'})+g(s^{'})}),\mathrm{rhs(s_{goal})=0} \tag{5}$$

Each node s in priority queue U is associated with a key-value pair k(s) ,be defined as

$$k(s) = [min(g(s), rhs(s) + h(s_{start}, s); min(g(s), rhs(s)] \tag{6}$$

Where h is the Euclidean distance, and the columns are arranged as follows:
k(s) 's dictionary order ascending sort

3.2.3. Smooth track

The path produced by the algorithm presented in this paper is represented as an ordered sequence of discrete nodes,P = {Pstart, P1, P2,..., Pend}. Yet despite meeting the specified multi-objective optimization criteria, the inter-node segments are, in most cases, straight-line connections, and this geometric form induces abrupt changes in curvature that do not conform to drone dynamic constraints. When such a path is executed directly, drastic fluctuations in velocity and acceleration are produced, energy expenditure rises, and the stability of data acquisition is correspondingly degraded. To mitigate these deficiencies, third-order uniform B-spline curves are adopted here for global-path smoothing, the aim being to secure C2continuity at the nodes [11] and, by doing so, reduce acceleration while improving flight smoothness.

Let the control-point sequence be denoted by Q0, Q1,..., Qn. Under this notation, the final point on the smoothed path, P(t), is given by:

$$P(t) = \sum_{i=0}^{n} Q_i B_{i,3}(t) t \in [0, 1] \tag{7}$$

A point P(t) on the curve is determined as the weighted average of the full set of control points Qi, the weights being prescribed by the basis function Bi,3(t), defined as follows:

$$\begin{cases} B_{0,3}(t) = \frac{1}{6}(-t^3 + 3t^2 - 3t + 1) \\ B_{1,3}(t) = \frac{1}{6}(3t^3 - 6t^2 + 4) \\ B_{2,3}(t) = \frac{1}{6}(-3t^3 + 3t^2 + 3t + 1) \\ B_{3,3}(t) = \frac{1}{6}t^3 \end{cases} \tag{8}$$

In the formula,Qi denotes a control point,that is,a three-dimensional coordinate expressed as a discrete path node generated by the algorithm. Along a given curve segment,"t"functions as the normalization parameter over the interval [0,1],determining positional variation. Bi,3(t),by contrast,denotes the cubic B-spline basis function—a fixed mathematical expression used to assign the corresponding weight.

In practical computation,each set of four adjacent control points defines a single curve segment; consideblue segment by segment,these are subsequently joined into a continuous and smooth trajectory. Particularly useful here is the method's local support property: if one control point is adjusted,only the associated local portion of the curve is affected,rather than the entire path being recomputed,a characteristic that makes the approach especially suitable for rapid replanning after

DOI: 10.54254/2755-2721/2026.33981

local obstacle avoidance. Within the resulting smoothed trajectory,both velocity and acceleration vary more gradually; correspondingly,peak acceleration is blueuced,energy loss remains constrained,and the operational duration of each flight mission is thereby extended.

3.3. Design of multi-machine collaborative data acquisition mechanism

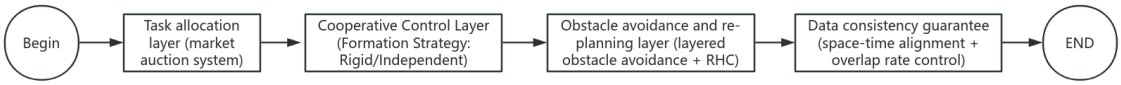


Figure 4. Core mechanism logic flowchart

3.3.1. Task allocation and collaborative control architecture

At the core of multi-machine collaborative data acquisition lies an efficient mechanism for task assignment and coordinated control. In the hierarchical hybrid architecture adopted in this study,initial task allocation and system-level coordination are managed by the ground station,whereas local coordination and dynamically adjusted task reallocation are executed by the machines through a self-organizing network.

Task Allocation Layer: Across the collection area,the operational space is divided into multiple sub-regions,after which task assignment is performed through an auction-based algorithm derived from market mechanisms [12]. For each sub-region,each drone computes a bid price as a function of its current position,remaining battery power,and sensor status. At the ground-station layer,all submitted bids are aggregated,and tasks are subsequently allocated to minimize total cost. Under large-scale operating conditions,a regional grid-based decentralized scheme is introduced; in this setting,the original target area is transformed into a set of standardized sub-regions,thereby enabling multiple drones to collaborate in collecting data from high-cost areas.

Coordinated Control Layer: adopted here is a formation-control strategy that combines the leader–follower approach with the virtual-structure method. Under open-area operating conditions,rigid formation flight is maintained to improve the consistency of data acquisition; within narrow-area segments,by contrast,the formation is divided into independent flight operations,with safe separation distances preserved through coordination among the aircraft.

3.3.2. Obstacle avoidance and real-time replanning strategy

In multi-drone collaborative settings,obstacle avoidance presents a genuinely dual-layer difficulty: environmental obstacles must be negotiated,and inter-drone collisions must be suppressed at the same time. To handle this coupled constraint structure,a hierarchical collaborative obstacle-avoidance framework is proposed:

Global obstacle avoidance: During the global planning stage,by exchanging environmental maps and flight plans,known static obstacles and inter-aircraft path conflicts are screened out in advance. For target allocation,the Hungarian algorithm is introduced so that trajectory crossings—and the downstream interference they often induce—are blueuced to the extent possible.

Local obstacle avoidance. During flight,once an unexpected obstacle is detected or,stated slightly differently,once the inter-drone distance falls below the prescribed safety threshold,local obstacle avoidance is activated. For this layer of avoidance computation,the RVO2 method (Speed Obstacle Method) is employed to derive the obstacle-avoidance velocity vector,with each drone carrying out

DOI: 10.54254/2755-2721/2026.33981

the calculation independently while coordination of the avoidance direction is maintained across agents [13].

Emergency obstacle avoidance. In cases where the preceding strategies still fail to realize effective avoidance,the emergency obstacle-avoidance mode is enteblue. Within the artificial potential field framework,a repulsive force field is introduced; from the obstacle position and relative velocity,an emergency avoidance force is then generated,allowing the system to exit the hazardous region with minimal delay.

Dynamic Replanning Strategy: Once obstacle-avoidance maneuvers displace a drone from its nominal route,replanning and recovery must begin immediately. In the present study,the Rolling Time-Domain Optimization (RHC) framework is adopted: at each planning cycle,a local trajectory spanning the next H steps is computed from the current state,while perceived environmental information and mission-level objectives are incorporated simultaneously [14]. Through this mechanism,a workable balance is achieved between planning optimality and real-time computational efficiency—a trade-off particularly well matched to dynamic urban environments.

3.3.3. Consistency assurance of co-collected data

For multi-machine collaborative acquisition,the endpoint is straightforward: multimodal data must remain consistent in both space and time. To secure that consistency,two measures are adopted in the present paper.

At the level of temporal-spatial registration,sub-millisecond synchronization across all drones is maintained through RTK-GPS-based coordination,with timestamps attached to the acquiblue data kept uniform from one platform to the next. Within the spatial reference layer,coordinates are normalized under the CGCS2000 system,thereby eliminating systematic positional deviations between drones (namely,the offsets that arise when separate platforms report location information under nonuniform reference settings).

During collaborative acquisition,overlapping-rate control is handled through inter-machine communication,real-time positional updates and acquisition-progress information being shablue continuously so that flight speed and route spacing can be adjusted on the fly,keeping the image-overlap rate between adjacent acquisition strips within the pblueefined 65%–85% range. Should an acquisition gap appear,or should overlap drop below the requiblue threshold,supplementary acquisition tasks are then triggered.

4. Data acquisition quality control and system verification

4.1. Experimental environment and multimodal data quality assessment system

4.1.1. Experimental environment

For an objective assessment of the proposed MO-RRT* algorithm,three scenario categories were recreated in a simulation environment,after which the resulting performance was compablue with that of the conventional A* algorithm and the standard Artificial Bee Colony (ABC) algorithm. Within the ROS + Gazebo simulation platform,the drone model was assigned sensor parameters identical to those measublue under real operating conditions. The platform configuration was specified as follows:

Drone model: using the DJI Jingwei M300 RTK as the reference platform,the system was equipped with a LiDAR unit (Livox AVIA),a 24 MP visible-light camera,and an RTK positioning

DOI: 10.54254/2755-2721/2026.33981

module,the corresponding sensor specifications being fully aligned with those of the physical hardware (that one-to-one consistency was maintained deliberately,rather than approximately,because the simulation was intended to mirror deployment conditions as closely as possible).

Within Gazebo,rigid-body dynamics,collision detection,and sensor-noise simulation are handled by the physics engine. For the gravitational component,acceleration was fixed at 9.8 m/s,whereas the air-resistance coefficient was calibrated to match low-altitude urban operating conditions.

As for scene reproduction,three-dimensional grid maps were constructed respectively for three representative urban scenarios:

High-rise building canyon zone: street width 15–25 m,building height 100–150 m,with GNSS signal obstruction zones explicitly designated;

Densely populated low-rise residential area: building heights of 20–50 m and inter-building spacing of 10–15 m,overhead pipelines and other irregular obstacles being incorporated into the environmental layout as additional constraints.

Open squares and public spaces: open ground areas with limited pedestrian traffic and temporary construction zones.

Computing platform: Intel Core i7-12700H CPU,32 GB RAM,Ubuntu 20.04 with ROS Noetic,and Gazebo 11.

For comparison,both the A* algorithm and the standard Artificial Bee Colony (ABC) algorithm were implemented in the same simulation environment,with parameter settings held consistent with those reported in the relevant literature.

In every experiment,the drone's initial position and destination were assigned through random initialization. For each run,path length,planning time,data quality score,and obstacle-avoidance success rate were recorded. Each scenario was repeated 30 times to blueuce run-to-run variation,and the results were summarized using mean values.

4.1.2. Point cloud data quality assessment

Point cloud data constitutes the basis of 3D reconstruction,and its quality is assessed along three dimensions:

Completeness refers to the extent to which the acquiblue point cloud covers the target area. Defined as the proportion of observed point-cloud volume relative to the total volume theoretically requiblue,this metric captures coverage in explicit volumetric terms. In urban environments,occlusion often leaves some regions unscanned; viewed in that light,completeness indicates whether critical parts of the dataset are missing.

Precision characterizes the deviation separating point-cloud coordinates from their corresponding true coordinates. Once ground control points have been established,their coordinates extracted from the point cloud,and these values set against the actually measublue coordinates,the root mean square error can be calculated. Within the overlapping zones of adjacent flight bands,relative precision can likewise be assessed from the residuals generated during point-cloud registration.

Density refers to the number of point-cloud points distributed over a unit area. For three-dimensional modeling,a minimum threshold of 100 points per square meter is ordinarily requiblue. By definition,this quantity is obtained by dividing the total number of point-cloud points by the projected area of the coveblue region. Of equal concern is density uniformity,since localized areas of excessive concentration or inadequate coverage are better avoided (both conditions,in practice,can degrade downstream modeling consistency).

DOI: 10.54254/2755-2721/2026.33981

4.1.3. Image data quality assessment

Image data provide the texture information on which 3D models rely,and the quality of those data directly conditions the visual realism of the model,along with the level of fine detail that can be represented. Against that methodological backdrop,the present paper focuses on the following image-quality parameters:

Light adaptation: Across urban scenes,illumination often changes abruptly,localized regions therefore appearing overexposed or,in other cases,underexposed. As an evaluative indicator,the balance of the image-brightness histogram distribution is used to quantify the deviation between an image's mean brightness and the ideal median value,while the proportion of highlight regions is also examined. During flight operations,exposure time and ISO are adjusted so that the histogram remains concentrated in the mid-tone range.

Overlapping Rate Control: For 3D reconstruction,a sufficiently high overlap between adjacent images is requiblue,the heading overlap generally being set to not less than 80% and the lateral overlap to not less than 60%. During path planning,explicit overlap constraints are imposed and,with real-time positional feedback incorporated,image-acquisition intervals are adjusted so that overlap remains within the preset bounds. From photographic geometry together with the real-time pose,the overlap rate is then computed.

Resolution matching requires the image ground sample distance (GSD) to align closely with point-cloud density; without such correspondence,texture-mapping accuracy deteriorates. GSD,by definition,is controlled by flight altitude and camera focal length,and for that reason flight altitude is adjusted dynamically within path-planning procedures—specifically according to scene importance and the underlying modeling requirements—to achieve adaptive resolution.

4.2. System experimental design and performance analysis

4.2.1. Experimental path comparison scheme

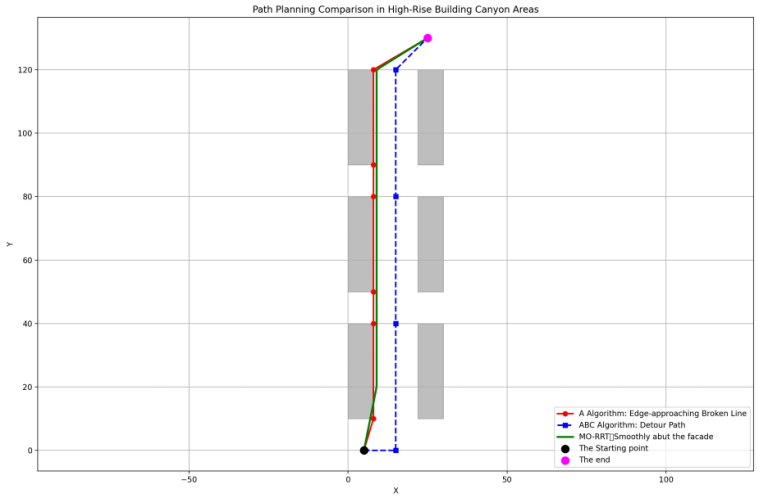


Figure 5. Comparative diagram of path planning for the three algorithms in the "high-rise building canyon area"

DOI: 10.54254/2755-2721/2026.33981

4.2.2. Comparative analysis of experimental results

(1) Comparison of Path Quality and Collection EfficiencyAcross the three evaluated scenarios,average algorithmic performance was documented over 30 independent runs. As shown in Table 2,the proposed MO-RRT* algorithm entails a slightly longer planning time per run than A (a gap traceable to the added computational burden associated with multi-objective optimization), yet,on both path length and data-quality metrics,it outperforms every comparison algorithm.

Table 2. Comparison table of path quality and collection efficiency across different scenario types

algorithm	Scene Type	Average route length(m)	Data Quality Score	Average planning time(s)	Obstacle avoidance success rate
A*	Valley area	356	0.72	0.5	92%
ABC		342	0.81	3.8	96%
MO-RRT*		328	0.89	2.1	99%
A*	Dense residential area	412	0.68	0.6	87%
ABC		398	0.77	4.3	92%
MO-RRT*		378	0.85	2.6	97%
A*	Open Square	285	0.75	0.5	96%
ABC		272	0.83	3.4	98%
MO-RRT*		265	0.91	1.9	99%

(3) Algorithm Convergence Analysis

Set against the convergence behavior of the standard ABC algorithm,the proposed multi-objective strategy for path-cost computation exhibits a distinctly faster optimization trajectory. In the figure cited below,the proposed method reaches an approximate optimum after about 15 iterations; not until nearly 30 iterations does the standard ABC algorithm draw close to a comparable solution. Read directly from that comparison,the inclusion of elite-population initialization,coupled with a guided search mechanism,appears to enhance convergence efficiency markedly.

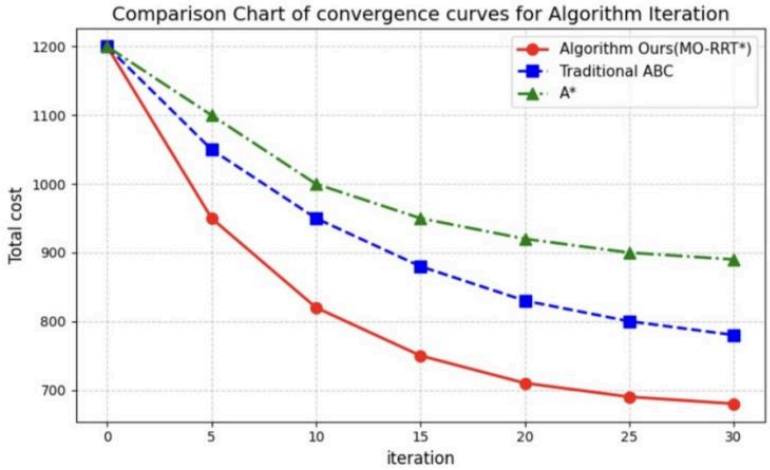


Figure 6. Comparison chart of algorithm iteration convergence curves

(4) Along the same path,a direct comparison was made between the speed-variation curves obtained with the conventional A* method and those generated by the proposed algorithm so as to

DOI: 10.54254/2755-2721/2026.33981

gauge how effectively trajectory smoothness is improved. As indicated in the figure,the proposed algorithm yields smoother speed transitions; acceleration,correspondingly,is blueuced to a marked extent,and energy consumption declines as a result. Within the smoothed trajectory produced by the proposed method,acceleration peaks are 32% lower,and the standard deviation of speed variation is blueuced by 28% relative to the traditional A* algorithm—evidence consistent with lower energy expenditure and,by extension,a longer flight duration.

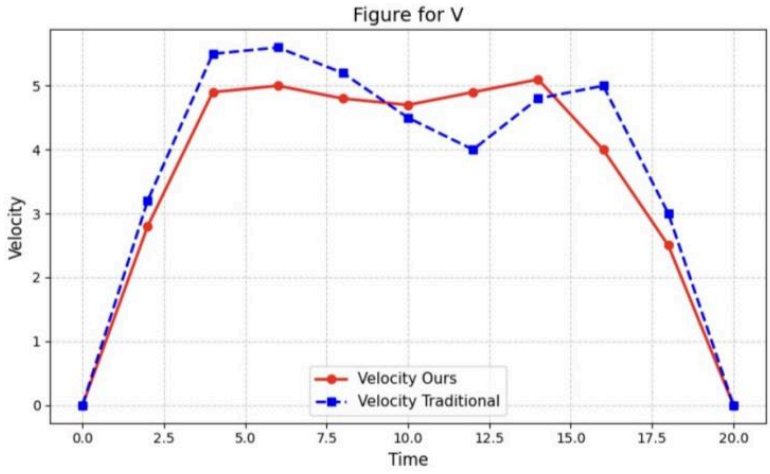


Figure 7. The curve showing the change in trajectory velocity before and after algorithmic smoothing

4.3. Verification of typical application scenarios based on simulation

This section tests whether the proposed acquisition system remains usable under differing operating conditions by reproducing representative application tasks within a simulation environment.

4.3.1. Real-scene 3D architectural modeling

Within the simulated high-rise building canyon scene,a 150 m supertall building was designated as the modeling target. Along the trajectory produced by the proposed system,data were collected and then imported into ContextCapture for 3D reconstruction [15]. When the reconstructed model was compared against the ground-truth data,planar accuracy reached 0.08 m,whereas elevation accuracy reached 0.15 m; as for the texture mapping,it remained clear and exhibited no visible distortion. Across the facade,structural features were preserved in a largely complete state,with no notable voids attributable to occlusion. Relative to conventional equidistant flight-path schemes,modeling efficiency increased by approximately 35%,a finding that points quite directly to the practical value of the proposed path-planning strategy for fine-grained modeling tasks.

4.3.2. Verification of security inspection tasks

Within simulated high-density residential scenes,security inspection operations are represented by the detection of unauthorized construction areas within specified buildings. For this task,inspection trajectories spanning rooftops and balconies are autonomously generated by the proposed system,real-time image data being transmitted throughout the flight process (that is,during route execution itself). Under the experimental conditions considered here,the algorithm reliably identifies

DOI: 10.54254/2755-2721/2026.33981

the predefined "suspected illegal construction" regions; compared with manually designed paths,route coverage improves by roughly 20%,while the missed-detection rate falls below 8%.

4.3.3. Verification of environmental monitoring tasks

Within the open-square simulation scene,the air-quality monitoring task is reproduced. Virtual gas sensors are mounted on the drone,concentration measurements being acquired through those sensors and then fused with a 3D point cloud to generate a spatial pollutant-distribution map. In the multi-drone collaborative data-collection experiments,the pattern is straightforward: relative to single-drone operation,the collaborative scheme improves monitoring efficiency by roughly 60%,while spatial resolution also increases.

5. Conclusion

5.1. Research work summary

This study examines a multi-modal drone data-acquisition system tailored to complex urban environments,and several results are central. (1) Hardware system: a multi-sensor integration platform was developed,PPS pulses being used for hardware-trigger synchronization, with the measublue synchronization error kept below 1 ms. For spatial calibration,a grid pattern was used in combination with the Kalibr tool,producing a reprojection error of under 1 pixel (a threshold that,in practical deployment terms,reflects closely aligned multi-sensor registration). (2) Path planning: a multi-objective path-planning method with embedded data-quality metrics was proposed,the core optimization function jointly balancing path length,threat cost,and data-quality cost. Within ROS/Gazebo simulation environments,and in direct comparison with both A* and the conventional ABC algorithm,the outcome pattern was unambiguous: under canyon-scenario conditions,the MO-RRT algorithm increased data-quality scores by 23.6% relative to A* and by 9.9% relative to ABC,while path length was blueuced by 7.9% and 4.1%,respectively. Briefly put,data quality improved as path cost declined.

For multi-drone collaboration,a task-allocation framework was developed on the basis of market-auction mechanisms together with hierarchical obstacle-avoidance coordination (that is,allocation and avoidance were handled in an integrated rather than separate manner). Under the simulation conditions,multi-drone operation yielded an efficiency gain of approximately 60% over single-drone systems in open-plaza monitoring tasks; in canyon-area data-collection tasks,point-cloud completeness reached 92.6% (a high-coverage result within the stated simulation setup).

Across three application scenarios—real-world 3D modeling,security inspection,and environmental monitoring—performance gains were repeatedly observed,although the magnitude of improvement varied by task. Relative to conventional flight trajectories,modeling efficiency increased by 35%,inspection coverage rose by 20%,missed-detection rates fell below 8%,and monitoring efficiency improved by 60%. Alongside these results,a technical scheme for campus-environment data acquisition and point-cloud fusion was also put forward,intended to serve as a reference point for subsequent real-world validation.

5.2. Future research directions

Real-world engineering validation stands as the immediately consequential next test: even though the present study confirms the algorithm's effectiveness under simulation conditions,actual urban

DOI: 10.54254/2755-2721/2026.33981

environments bring additional sources of uncertainty into play—dynamic obstacles,weather variability,and signal interference among them (conditions under which idealized assumptions,in practice,rarely hold for long). In the next phase,collaborative data-acquisition experiments using drones and handheld scanners are planned for campus and industrial-park settings,the objective being to test the system's practical applicability under operational conditions.

For multi-source point-cloud fusion,processing will be carried out with software such as Cyclone3D,thus allowing a more searching evaluation of point-cloud completeness and modeling accuracy. Beyond the fusion pipeline proper,the research advances toward edge intelligence and real-time AI deployment, extending to lightweight airborne neural networks for real-time object detection and anomaly alerting,together with 5G/6G-enabled cloud-edge-end collaboration intended to support large-scale real-time operations.

Under extreme-environment requirements,strengthened drone adaptability is paired with anti-interference communication and all-weather sensing modules—millimeter-wave radar and thermal infrablue cameras,in particular—so that system robustness can be improved under adverse conditions such as rain,snow,haze,and strong electromagnetic interference.

Drawing on cutting-edge technologies and the GigaVision dataset,the research supports large-scale 3D reconstruction of relevant scenarios; it also investigates the use of the DeepMIMO dataset within integrated communication-and-perception systems; and,from that basis,extends toward application domains including disaster emergency response and high-precision map acquisition for autonomous driving.

References

[1] Mohsan S A H, et al. Unmanned aerial vehicles (UAVs): A survey on civil applications and key research challenges [J]. IEEE Access, 2022, 10: 98734-98763.
[2] Pajares, G. Overview and current status of remote sensing applications based on unmanned aerial vehicles (UAVs). Photogrammetric Engineering & Remote Sensing, 2015, 81(4), 281-330.
[3] Zhu J, Ren K, Fu C, et al. Online camera-lidar calibration with sensor fusion [J]. IEEE Robotics and Automation Letters, 2021, 6(2): 1826-1833.
[4] Geiger A, Moosmann F, Car Ö, et al. Automatic camera and range sensor calibration using a single shot [C]//2012 IEEE International Conference on Robotics and Automation (ICRA). IEEE, 2012: 3936-3943.
[5] Wang H, Guo Y, Yang J, et al. A survey of path planning algorithms for unmanned aerial vehicles in complex environments [J]. IEEE Access, 2021, 9: 119326-119348.
[6] Zhou T., Tucker R., Flynn J., et al. GigaMVS: A benchmark for ultra-large-scale multi-view stereo [C] // Proceedings of the 2024 IEEE/CVF Conference on Computer Vision and Pattern Recognition (CVPR). IEEE, 2024.
[7] Q. Zhu, J. Huang, and Z. Hu, "A novel multi-sensor fusion approach for UAV navigation under GNSS-denied conditions, " IEEE Trans. Veh. Technol., vol. 70, no. 9, pp. 8728–8740, Sep. 2021.
[8] J. Rehder, J. Nikolic, T. Schneider, T. Hinzmann, and R. Siegwart, "Extending kalibr: Calibration of large-scale multi-sensor systems, " in Proc. IEEE Int. Conf. Robot. Autom. (ICRA), 2016, pp. 3591–3597.
[9] O. Arslan and P. Tsiotras, "Multi-objective trajectory planning for UAVs using RRT* and weighted sum optimization, " J. Intell. Robot. Syst., vol. 96, no. 1, pp. 65–79, Oct. 2019.
[10] M. K. Al-Shabi and Z. A. Al-Yemeni, "Elite-guided artificial bee colony algorithm for global optimization, " Swarm Evol. Comput., vol. 68, p. 101014, Jan. 2022.
[11] F. Gao, L. Wang, K. Wang, W. Wu, and S. Shen, "Optimal trajectory generation for quadrotors through flatness transformation and time allocation, " IEEE Trans. Robot., vol. 37, no. 3, pp. 856–869, Jun. 2021.
[12] H. Zhao, F. Gao, and J. Pan, "Auction-based distributed task allocation for multi-UAV systems in urban environments, " IEEE Transactions on Automation Science and Engineering, vol. 19, no. 4, pp. 2971–2984, Oct. 2022.
[13] S. Liu, M. Watterson, K. Mohta, and V. Kumar, "Collision-avoiding trajectory planning for multi-robot systems using reciprocal velocity obstacles, " Int. J. Robot. Res., vol. 37, no. 13–14, pp. 1609–1633, Dec. 2018.

DOI: 10.54254/2755-2721/2026.33981

[14] Y. Lin, X. Huang, and R. Xiong, "Model predictive control for multi-UAV cooperative sensing with guaranteed data consistency, " IEEE Transactions on Cybernetics, vol. 52, no. 8, pp. 7750–7762, Aug. 2022.
[15] A. L. Majdik, D. Verda, and D. Scaramuzza, "Air-ground collaborative 3D reconstruction using vision-based SLAM and mesh refinement, " IEEE Robot. Autom. Lett., vol. 5, no. 4, pp. 6189–6196, Oct. 2020.